






## **Deterministic one-way logic gates on a cloud quantum computer**

Downloaded from: <https://research.chalmers.se>, 2024-06-29 15:22 UTC

Citation for the original published paper (version of record):

Yang, Z., Ku, H., Baishya, A. et al (2022). Deterministic one-way logic gates on a cloud quantum computer. *Physical Review A*, 105(4). <http://dx.doi.org/10.1103/PhysRevA.105.042610>

N.B. When citing this work, cite the original published paper.

**Deterministic one-way logic gates on a cloud quantum computer**Zhi-Peng Yang <sup>1,2</sup>, Huan-Yu Ku,<sup>2,3,\*</sup> Alakesh Baishya,<sup>2</sup> Yu-Ran Zhang <sup>2</sup>, Anton Frisk Kockum,<sup>4</sup> Yueh-Nan Chen,<sup>2,3</sup>  
Fu-Li Li,<sup>1,†</sup> Jaw-Shen Tsai,<sup>5,6</sup> and Franco Nori <sup>2,6,7,‡</sup><sup>1</sup>*Ministry of Education Key Laboratory for Nonequilibrium Synthesis and Modulation of Condensed Matter, Shaanxi Province Key Laboratory of Quantum Information and Quantum Optoelectronic Devices, School of Physics, Xi'an Jiaotong University, Xi'an, Shaanxi 710049, China*<sup>2</sup>*Theoretical Quantum Physics Laboratory, RIKEN Cluster for Pioneering Research, Wako-shi, Saitama 351-0198, Japan*<sup>3</sup>*Department of Physics and Center for Quantum Frontiers of Research and Technology (QFort), National Cheng Kung University, Tainan 701, Taiwan*<sup>4</sup>*Department of Microtechnology and Nanoscience, Chalmers University of Technology, 412 96 Gothenburg, Sweden*<sup>5</sup>*Department of Physics, Tokyo University of Science, Shinjuku, Tokyo 162-0825, Japan*<sup>6</sup>*RIKEN Center for Quantum Computing, Wako-shi, Saitama 351-0198, Japan*<sup>7</sup>*Department of Physics, The University of Michigan, Ann Arbor, Michigan 48109, USA*

(Received 5 January 2022; accepted 23 March 2022; published 18 April 2022)

One-way quantum computing is a promising candidate for fault-tolerant quantum computing. Here, we propose protocols to realize a deterministic one-way controlled-NOT (CNOT) gate and one-way  $X$  rotations on current quantum-computing platforms. By applying a delayed-choice scheme, we overcome a limit of most currently available quantum computers, which are unable to implement further operations on measured qubits or operations conditioned on measurement results from other qubits. Moreover, we decrease the error rate of the one-way logic gates, compared to the original protocol using local operations and classical communication. In addition, we apply our deterministic one-way CNOT gate in the Deutsch-Jozsa algorithm to show the feasibility of our proposal. We demonstrate all these one-way gates and algorithms by running experiments on the cloud quantum-computing platform IBM Quantum Experience.

DOI: [10.1103/PhysRevA.105.042610](https://doi.org/10.1103/PhysRevA.105.042610)**I. INTRODUCTION**

Measurement-based one-way quantum computing [1–3], where single-qubit operations and measurements are applied to an initial highly entangled cluster state or graph state [4,5], is considered a promising candidate for quantum computation. This approach to quantum computing is potentially more robust against noise and errors than the quantum circuit model, due to advantages in implementing fault-tolerant quantum computing [6–9]. Recently, several proposals for combining one-way quantum computing with quantum error correction and quantum algorithms have been presented [10–13]. Unlike circuit-based quantum computing, in which the scale of the quantum computer is limited by the number of available qubits and gates, measurement-based quantum computing is restricted by the scale of the cluster state one can generate [13]. Large two-dimensional cluster states have been generated in experiments with photonic qubits [14–18].

The ideas of cluster states and one-way quantum computing were proposed two decades ago. The earliest works on one-way quantum computing and cluster states applied to solid-state qubits and superconducting circuits were consid-

ered in Refs. [19–21]. Moreover, a large variety of protocols on a series of one-way logic gates have been proposed and implemented, including single-qubit, two-qubit, and multi-qubit logic gates, e.g., the TOFFOLI gate and the CARRY gate [22–29]. Moreover, there have been a number of experiments generating cluster states, and constructing one-way quantum logic gates, performed in optical systems [14,15,27,30–37], trapped ions [38], and nuclear magnetic resonance (NMR) systems [39].

Recently, superconducting qubits (e.g., [40–45]) have attracted significant attention for quantum computing due to their scalability and controllability. The superconducting platform is considered as one of the most promising for building universal quantum computers, as exemplified by, e.g., commercial devices, including IBM's [46–49] and Google's [50,51] superconducting processors. A series of theoretical and experimental protocols for generating cluster states of superconducting qubits have been presented in [19–21,52–59], as well as theoretical protocols [2,29] for one-way logic gates in superconducting processors. However, experimental demonstrations of one-way quantum computing in superconducting systems were lacking until very recently [60,61].

In this paper, we demonstrate deterministic one-way quantum computing using the IBM Quantum Experience (IBMQ). The IBMQ contains a series of quantum chips composed of superconducting qubits, which can be used to construct quantum logical circuits consisting of quantum logic gates. As an

\*huan\_yu@phys.ncku.edu.tw

†fli@xjtu.edu.cn

‡fnori@riken.jp

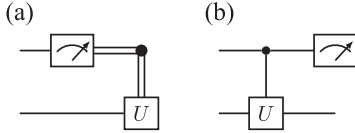


FIG. 1. Circuits for (a) a classically conditioned (the double line corresponds to classical communication) operation  $U$  and (b) the delayed-choice approach for the same operation. We consider a situation where  $U$  only acts on the second qubit when the outcome of the measurement on the first qubit is 1. For such  $U$ , these two circuits yield the same outcome.

on-cloud quantum computing service, IBMQ provides users with a powerful platform for experimentally implementing not only fundamental quantum phenomena [62–65] but also quantum information processing tasks [47,49,66–70]. However, until very recently [71], due to the limitation of the physical structure of the IBMQ chips, they did not provide sufficient functionality to directly test many concepts of one-way quantum logic gates. For instance, the IBM devices were not able to enact qubit operations conditioned on the results of qubit measurements. To the best of our knowledge, this remains the case for other quantum-computing systems.

We therefore introduce a protocol based on replacing the quantum operations conditioned on the measurement results [the “local operations and classical communication” (LOCC) approach] with delaying the choice of the measurement (the delayed-choice approach; see Fig. 1). Although we need additional entangling gates to implement this delayed-choice approach, it opens the way for experimental tests of many important concepts in one-way quantum computing.

We experimentally construct a deterministic one-way two-qubit gate [the one-way controlled-NOT (CNOT) gate] and also use it to implement the Deutsch-Jozsa (DJ) algorithm [72,73] on a five-qubit chip called IBMQ Lima. Note that here “deterministic” means that the one-way logic gate has a fixed output; for a “nondeterministic” one-way logic gate, a feed-forward operation is required after measuring and obtaining the output. In the following, as we are not going to discuss nondeterministic one-way logic gates, for brevity we will omit “deterministic.”

For the one-way CNOT gate, the measurement bases on the cluster state are fixed, while for most single-qubit one-way logic gates the measurement bases of one subsystem are determined by the measurement results from another subsystem (LOCC). Therefore, implementing a one-way logic gate requires performing measurements at different times, and the feedback of measurement results can also introduce errors [1,2]. By applying the delayed-choice method, one-way logic gates can be achieved with simultaneous measurements on the entire cluster state. We can thus significantly decrease the errors from measurements and feedback operations. As an explicit example, we investigate the one-way  $X$ -rotation gate. With our approach, superconducting qubits become more amenable to one-way quantum computing.

This paper is organized as follows. In Sec. II, we introduce the replacement of the quantum operation conditional on the classical measurement result with delayed choice of the measurement. With this approach, we can experimentally realize a

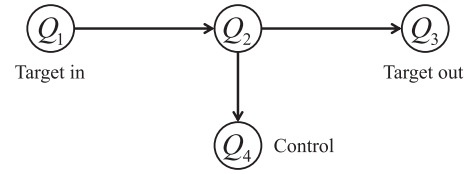


FIG. 2. Schematic illustration of the setup for the one-way CNOT gate. The full system consists of four qubits. Qubits  $Q_1$ ,  $Q_3$ , and  $Q_4$  act as the input target state, the output target state, and the control, respectively. The arrows represent standard controlled-Z gates, which start at the control qubit and end at the target qubit.

one-way CNOT gate. We also apply the one-way CNOT gate in the DJ algorithm on the five-qubit IBMQ Lima. In Sec. III, we show the advantage of considering the delayed choice of the measurement and experimentally present the one-way  $X$ -rotation gate. Finally, in Sec. IV, we briefly summarize our results and discuss limitations for the possibility of developing one-way quantum computing on quantum processors.

## II. CONSTRUCTION AND APPLICATION OF THE ONE-WAY CNOT GATE

### A. The standard one-way CNOT gate

We start by briefly recalling how to construct the cluster state for implementing a one-way CNOT gate [1,2]. The system, consisting of four qubits ( $Q_1$ ,  $Q_2$ ,  $Q_3$ , and  $Q_4$ ; see Fig. 2), is first prepared in the state

$$|\Psi\rangle_{\text{in}}^{\text{CNOT}} = |\psi\rangle_1 |+\rangle_2 |+\rangle_3 |\phi\rangle_4, \quad (1)$$

where  $|\pm_x\rangle$  is the eigenstate of the Pauli  $X$  matrix with the eigenvalue  $\pm 1$ . The subscripts in Eq. (1) are used to denote the physical qubits. Here,  $|\psi\rangle_1$  and  $|\phi\rangle_4$  are the input target state and control state, respectively, of the CNOT gate, while  $Q_3$  plays the role of the output target state. More specifically, if  $|\phi\rangle_4 = |1\rangle_4$ , the  $X$  operation is carried out on the “transferred” state  $|\psi\rangle_3$ .

The above initialization process can be achieved by implementing suitable single-qubit logic gates. After the initialization, we sequentially apply a series of controlled-Z (CZ) gates  $C_Z^{(12)}$ ,  $C_Z^{(23)}$ , and  $C_Z^{(24)}$  to prepare the cluster state [2,29]. Here,  $C_Z^{(ij)}$  represents a CZ gate with  $i$  and  $j$  labeling the control and target qubits, respectively. The full initialization circuit is shown in the left part of Fig. 3(a).

After constructing the cluster state, we simultaneously measure  $X$  on  $Q_1$  and  $Q_2$  with the results  $s_1$  and  $s_2$ , respectively. Here, we use the notation  $s_i = 0$  ( $s_i = 1$ ) to denote the corresponding outcome of the  $i$ th qubit with the eigenvalue  $+1$  ( $-1$ ) of the Pauli  $X$  matrix. Finally, to realize deterministic one-way quantum computing, a feedforward operation,

$$U_{\Sigma}^{\text{CNOT}} = Z_3^{s_1+1} X_3^{s_2} \otimes Z_4^{s_1}, \quad (2)$$

is applied on  $Q_3$  and  $Q_4$ . Here,  $\alpha_j$  ( $\alpha = X, Y, Z$ ) denotes the corresponding Pauli operation acting on qubit  $j$ . Each operation in Eq. (2) is conditioned on the measurement results, which are transferred with classical communication. Note that for implementing the one-way CNOT gate the measurement bases of the subsystems are always fixed.

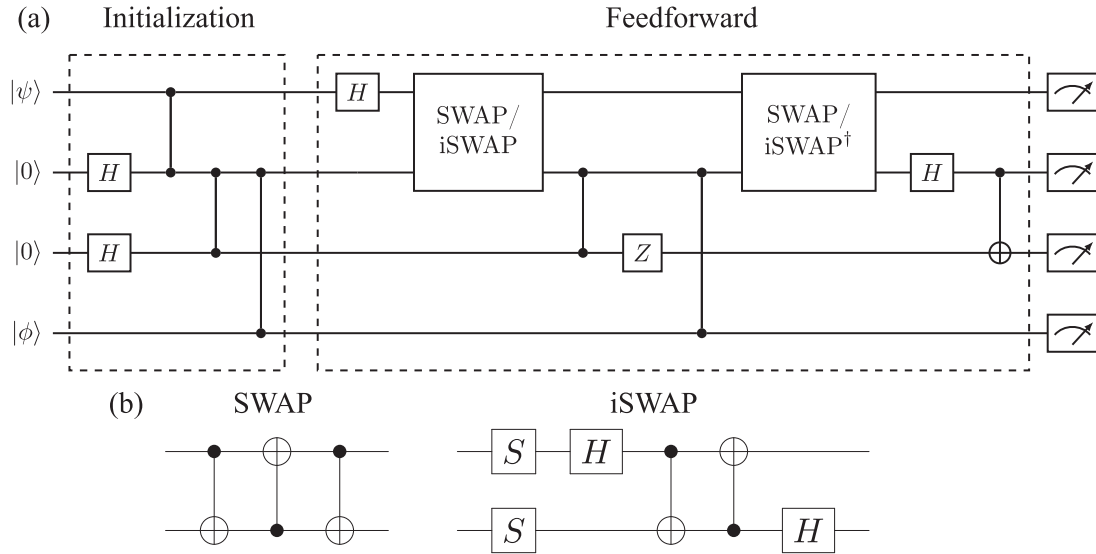


FIG. 3. (a) The circuit for constructing the delayed-choice one-way CNOT gate on the IBMQ Lima with the first and fourth qubits being the input target and the control, respectively. The output target is the third qubit. Here the SWAP gates or ISWAP gates are inserted due to the limited connectivity of the IBMQ Lima. (b) The gate decomposition of the SWAP gate and the ISWAP gate into CNOT gates (the native two-qubit gate of IBMQ devices) and single-qubit gates.

### B. Construction of the delayed-choice one-way CNOT gate with IBMQ Lima

In this section, we experimentally implement the delayed-choice one-way CNOT gate using the IBMQ Lima, which is a five-qubit chip having a similar layout as Fig. 2, with another ancilla qubit  $Q_5$  added below  $Q_4$ . The circuit for the one-way CNOT gate on IBMQ Lima is shown in Fig. 3.

Although the standard method of realizing a one-way gate can be experimentally implemented in many physical systems, including optical systems, trapped ions, and NMR [27,30,32–39], superconducting systems like IBMQ could not (until very recently [71]) directly apply the same strategy to achieve a one-way CNOT gate, due to a major limitation: Conditional operations, based on classical transfer of readouts, are forbidden. These “missing” functions prohibit the feedforward operation. To overcome these limitations, we apply the quantum delayed-choice method to replace the classical conditional operations.

In general, the quantum delayed-choice approach enables us to create a superposition of eigenstates, corresponding to all the possible readouts, and the superposed state collapses to the required eigenstate after the measurement operations. In this way, classical conditional operations can be replaced by CZ or CNOT operations, which are available on IBMQ devices. By relaxing the requirement that all operations following the initial entangling step should be single-qubit gates and measurements, we can now test many concepts and applications in the current IBM devices. Moreover, we can also analyze the effect of the error mitigation on the one-way computation (see also the later example). We note that the delayed-choice approach does not make any additional assumption of functionality for one-way quantum computing on the superconducting platform, since all the required operations can be carried out before measuring any qubit, such that we can consider this as a part of the cluster-state generation.

We now describe in detail the circuit model for the delayed-choice one-way CNOT operation. As mentioned above, the cluster state can be constructed by sequentially applying  $C_Z^{(12)}$ ,  $C_Z^{(23)}$ , and  $C_Z^{(24)}$  on the initial state given in Eq. (1). Before the delayed-choice operation, we first perform the Hadamard gate on  $Q_1$  to transfer the measurement basis from Z to X. Then, a SWAP or ISWAP gate is applied to exchange the quantum states of  $Q_1$  and  $Q_2$ , due to the architecture of IBM Lima.

Note that a SWAP gate can be decomposed into three CNOT gates, while an ISWAP gate is constructed by two CNOT gates and four single-qubit gates, as shown in Fig. 3(b). In this way, we can decrease the gate error by replacing SWAP gates with ISWAP gates, because the CNOT gate in general introduces more error than single-qubit gates.

Next, we implement the delayed choice of  $U_1 = Z_3^{s_1+1}$  and  $U_3 = Z_4^{s_1}$ , by applying  $C_Z^{(23)}$  followed by  $Z_3$ , and  $C_Z^{(24)}$ , respectively. After the delayed choice of  $U_1$  and  $U_3$ , the inverse of the SWAP or ISWAP operation is performed on  $Q_1$  and  $Q_2$ . Finally, a Hadamard gate, following the delayed choice of  $U_2 = X_3^{s_2}$ , is implemented.

To study whether ISWAP gates can reduce the noise from gate errors and the intrinsic environment interaction, we consider three different scenarios: (i) the delayed-choice one-way CNOT gate with SWAP gates, (ii) the delayed-choice one-way CNOT gate with ISWAP gates, and (iii) the delayed-choice one-way CNOT gate with ISWAP gates and error mitigation.

Here, we use the simplest error mitigation method provided by IBMQ [48,74–77]. In short, before experimentally implementing the delayed-choice CNOT gate, we test the results of Z measurements with the inputs being its eigenstates. The difference between ideal and tested results provides an error matrix which is used for error mitigation.

The experimental results from IBMQ Lima are presented in Fig. 4. To increase the transparency of the results, postprocessing is performed by summing the results of  $Q_1$  and  $Q_2$ ,

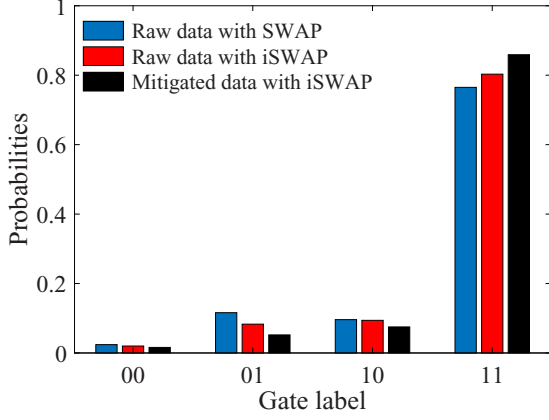


FIG. 4. Results of the one-way CNOT gate with inputs  $|0\rangle$  (target) and  $|1\rangle$  (control). The theoretical prediction of the output after the postprocessing is  $|11\rangle$ . The blue, red, and black bars correspond to using SWAP, ISWAP, and ISWAP with error mitigation, respectively.

because (i) theoretically the results of  $Q_1$  and  $Q_2$  are uniform in the delayed-choice one-way CNOT gate and (ii)  $Q_3$  and  $Q_4$  play the roles of the output of the target qubit and the controlled qubit, respectively, in the standard CNOT gate. In other words, we only need to access the results of  $Q_3$  and  $Q_4$  to see whether the delayed-choice one-way CNOT gate functions successfully.

Here, we only consider the case where the inputs of the control qubit and the target qubit are  $|1\rangle$  and  $|0\rangle$ , respectively. Thus, the output of the target qubit should be  $|1\rangle$ . The experimental results for all the different inputs are shown in Appendix A. We find that the experimental result with ISWAP gates outperforms the one with SWAP gates, which we expected since the sequence with ISWAP gates is less likely to introduce errors, as discussed above. Moreover, the error mitigation further improves the experimental results. In addition, we also apply quantum process tomography to compute the gate fidelity in terms of the Choi representation, namely,

$$F(G_1, G_2) = \text{tr}(\sqrt{\sqrt{\rho_{G_1}}\rho_{G_2}\sqrt{\rho_{G_1}}})^2, \quad (3)$$

where

$$\rho_{G_i} = (\mathbb{1} \otimes G_i)|\Psi\rangle\langle\Psi| \quad (4)$$

is the Choi state of the quantum operation  $G_i$  with  $|\Psi\rangle = \sum_i 1/\sqrt{d}|ii\rangle$  being the maximally entangled state. Here,  $d$  is the dimension of the local system. The experimental fidelities are, respectively, 0.804, 0.808, and 0.857, for the three different scenarios.

The device parameters of the IBMQ Lima superconducting processor used in our experiment are as follows. The average  $T_1$  and  $T_2$  of IBMQ Lima are 95.86 and 99.21  $\mu\text{s}$ , which represents the energy decay time and dephasing time of the qubits, respectively. The average two-qubit gate error rate  $\lambda$  (also called the two-qubit Clifford gate error rate) and gate time are approximately 1.1% and 405 ns, respectively. The average readout error is approximately 3% with a readout time around 5  $\mu\text{s}$ . In our simulation model, the error, introduced by the two-qubit gate, plays a significant role in our system. This is because the gate time and gate error of the two-qubit

gate are both one order of magnitude greater than those of the single-qubit gates. We note that these parameters vary over time, and the details of the parameters used in this paper are presented in Appendix A.

Here, we analyze each aforementioned error by some well-established models. We note that each model within our analysis is also used in the quantum assembly (QASM) simulator provided by the IBMQ library. The impact of qubit decoherence on the system obeys the quantum master equation:

$$\begin{aligned} \frac{d\rho}{dt} = & \sum_{i=1}^4 \frac{\kappa_1^i}{2} [2\sigma_-^i \rho \sigma_+^i - \sigma_+^i \sigma_-^i \rho - \rho \sigma_+^i \sigma_-^i] \\ & + \sum_{i=1}^4 \frac{\kappa_\phi^i}{4} [2\sigma_z^i \rho \sigma_z^i - 2\rho], \end{aligned} \quad (5)$$

where  $\rho$  is the density matrix,  $\sigma_+^i$  ( $\sigma_-^i$ ) denotes the creation (annihilation) operator, and  $\sigma_z^i$  represents the Pauli Z operator. Here, the parameters  $\kappa_1^i = 1/T_1^i$  and  $\kappa_\phi^i = 1/T_\phi^i$  are determined by the relaxation and pure dephasing times, respectively, where  $1/T_2 = 1/(2T_1) + 1/T_\phi$ . The delayed-choice one-way CNOT gates with SWAP gates and ISWAP gates require 12 and 10 two-qubit gates, respectively, and all the qubits are measured simultaneously. Thus, taking readout time into consideration, the total time to carry out the one-way CNOT gate is approximately 10  $\mu\text{s}$ . This brings the system a decoherence error rate of around 4%.

Here, we consider the effect of the gate error. In the quantum assembly simulator, the gate error of an  $n$ -qubit gate is described by an  $n$ -qubit depolarization error:

$$E_G(\lambda_G)\rho = (1 - \lambda_G)\rho + \lambda_G \frac{I}{2^n}, \quad (6)$$

where  $\lambda_G$  is the error rate. Inserting the number of CNOT gates and the two-qubit error rate, we obtain a error of approximately 10%. We note that the gate error is deduced from randomized benchmarking [78,79], where the two-qubit gate error rate represents the imperfection of both the single-qubit and CNOT gates.

Finally, we consider the effect of the readout error. The single-qubit readout error on a qubit can be described by probabilities  $\lambda_{01}$  and  $\lambda_{10}$ . Here,  $\lambda_{01}$  ( $\lambda_{10}$ ) is the probability of recording a noisy measurement outcome as 1 (0) given the ideal measurement outcome was 0 (1). According to the simulation result on the QASM simulator, the readout error of the two output qubits leads to an additional error rate of approximately 10%. We note that the above three models are considered independently by inserting the system's parameters into the simulations.

As a result, the main factors of noises, interfering with the operation of the delayed-choice one-way CNOT gate, are gate error and readout error. Either one leads to an error rate of around 10%. We recall that the decoherence of qubits causes an additional error rate of around 4%. Moreover, the total error can be reduced by applying measurement error mitigation. Our simulation fits the corresponding experimental results in Table I. All the estimated error rates are obtained via simulation on the QASM simulator, using the parameters of the IBMQ Lima.

TABLE I. Probability distribution for the delayed-choice one-way CNOT gate implemented on IBMQ Lima. Here, “Input  $|ij\rangle$ ” represents that the inputs of the target state and the control state are  $|i\rangle$  and  $|j\rangle$ , respectively. The  $|kl\rangle$  in the second to fifth column denotes the measurement with results  $kl$ .

Input $ 00\rangle$	$ 00\rangle$	$ 01\rangle$	$ 10\rangle$	$ 11\rangle$
Raw/SWAP	0.787	0.096	0.090	0.026
Raw/ISWAP	0.848	0.071	0.067	0.014
Mitigated/ISWAP	0.866	0.063	0.057	0.013
Input $ 01\rangle$	$ 00\rangle$	$ 01\rangle$	$ 10\rangle$	$ 11\rangle$
Raw/SWAP	0.025	0.108	0.110	0.757
Raw/ISWAP	0.018	0.089	0.099	0.794
Mitigated/ISWAP	0.012	0.052	0.075	0.860
Input $ 10\rangle$	$ 00\rangle$	$ 01\rangle$	$ 10\rangle$	$ 11\rangle$
Raw/SWAP	0.119	0.779	0.024	0.078
Raw/ISWAP	0.095	0.837	0.015	0.053
Mitigated/ISWAP	0.069	0.871	0.013	0.048
Input $ 11\rangle$	$ 00\rangle$	$ 01\rangle$	$ 10\rangle$	$ 11\rangle$
Raw/SWAP	0.125	0.023	0.748	0.104
Raw/ISWAP	0.096	0.016	0.811	0.077
Mitigated/ISWAP	0.061	0.013	0.854	0.072

**C. Implementing the Deutsch-Jozsa algorithm using the delayed-choice one-way CNOT gate**

After successfully constructing the delayed-choice one-way CNOT gate, we implement a practical DJ quantum algorithm [72,73] with this operation to show how our one-way CNOT gate works in practical problems.

The DJ algorithm is the first quantum algorithm ever invented. It finds out whether an  $n$ -bit Boolean function  $f(x) : \{0, 1\}^n \rightarrow \{0, 1\}$  with  $\{x \in R | 0 \leq x \leq 2^{n-1} |n\}$  is balanced or constant. Here, a constant function means that the result remains unchanged with arbitrary input, while for a balanced function half of the possible inputs yield the result zero, and the other half yield the result 1. A classical algorithm requires  $(2^{n-1} + 1)$  queries to distinguish the two types of functions, but the DJ algorithm can complete the process with a single query.

The logical process of the DJ algorithm is as follows [see also Fig. 5(a)]: To classify an  $n$ -bit Boolean function, we first initialize all  $n$  qubits (representing the input  $x$  of the function) in  $|0\rangle$ . An ancilla qubit  $q_{n+1}$  is prepared in  $|1\rangle$ . Then, Hadamard gates are applied on all qubits. Denoting the state of the ancilla qubit by  $|y\rangle$ , an oracle is implemented which maps  $|x\rangle|y\rangle$  to  $|x\rangle|y \oplus f(x)\rangle$ . Finally, we measure all  $n$  qubits in the  $X$  basis, which is achieved by inserting Hadamard gates before measuring  $Z$ . If the final outcome sums up to 1, the corresponding function  $f(x)$  is balanced, otherwise the function is constant. The explicit circuits for the constant function  $f(x) = 0$  and the balanced function  $f(x) = x$ , using the delayed-choice one-way CNOT gates, are presented in Figs. 5(b) and 5(c), respectively.

Figure 6 shows experimental results for distinguishing the balanced [ $f(x) = 0$ ] and constant [ $f(x) = x$ ] functions, respectively, by the DJ algorithm with the delayed-choice one-way CNOT gate. These results are also obtained on

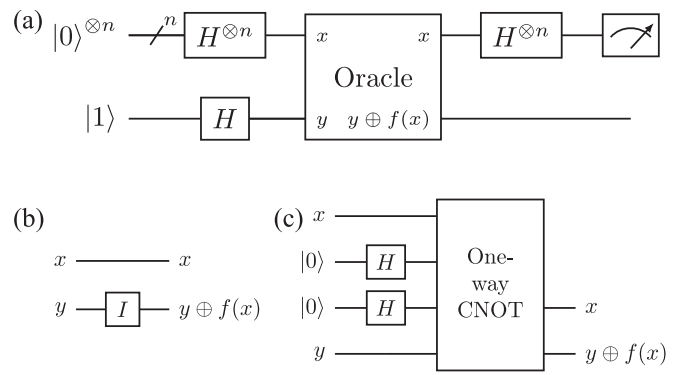


FIG. 5. Circuits for the DJ algorithm with the delayed-choice one-way CNOT gate. (a) The fundamental circuit representation of the  $n$ -bit DJ algorithm. The first  $n$  qubits are all prepared in  $|0\rangle$  while the ancilla qubit is prepared in  $|1\rangle$ . (b) The circuit representation of a 1-bit Boolean function with  $f(x) = 0$ . (c) The circuit representation of a 1-bit Boolean function with  $f(x) = x$ .

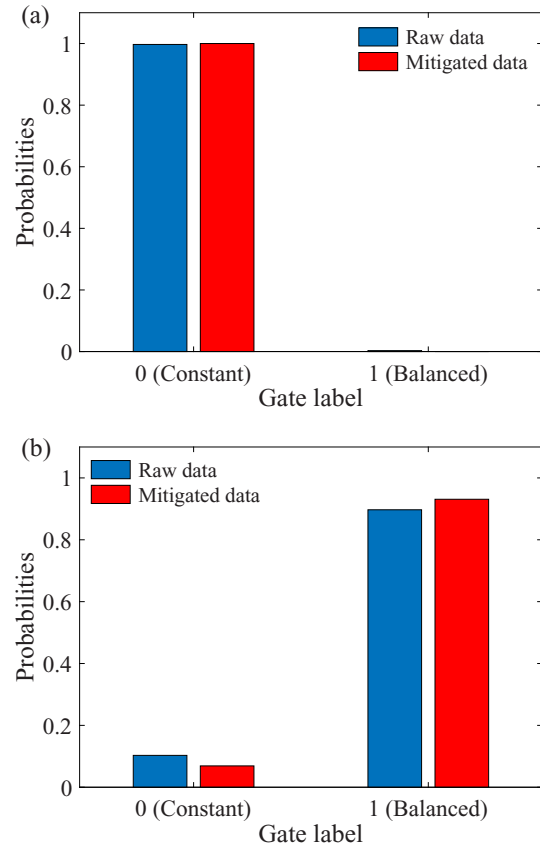


FIG. 6. Results for running the DJ algorithm on IBMQ Lima with (a) the constant function  $f(x) = 0$  and (b) the balanced function  $f(x) = x$ . In (b), we apply the delayed-choice one-way CNOT gate in the oracle [see Fig. 5(c)]. The blue and red bars correspond to results with and without measurement-error mitigation, respectively. When the measurement result is zero, the function is classified as constant. Otherwise it is classified as balanced.

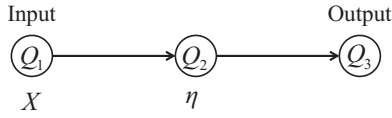


FIG. 7. The basic idea of the one-way  $X$ -rotation gate. The qubits  $Q_1$  and  $Q_3$  are the input and output qubits, respectively, and the arrows represent the standard CZ gates, which start at the control qubit and end at the target qubit. Here, the  $X$  under qubit  $Q_1$  represents that qubit  $Q_1$  is measured in the  $X$  basis, and the  $\eta$  under qubit  $Q_2$  represents the measurement basis of qubit  $Q_2$ , which is in the  $xy$  plane with an angle  $\eta$  to the  $x$  axis.

IBMQ Lima. Although the probability distributions are not equivalent to the theoretical predictions due to inevitable noise, our experimental results still show how the DJ algorithm works for the discrimination problem. In particular, for the balanced function, while the success probability  $p(0) < 1$ , it is significantly higher than the probability  $p(1)$  of the wrong answer. We note that, for the DJ algorithm, one would not need the success probability to be unity. In other words, the balanced and constant functions can be discriminated as long as the corresponding success probability is higher than the fail probability. Our experimental results satisfy this criterion by a wide margin.

### III. CONSTRUCTION OF THE DELAYED-CHOICE ONE-WAY $X$ -ROTATION GATE

As we attempt to develop a universal set of one-way logic gates, we need to construct single-qubit rotation gates, in addition to the entangling two-qubit gate demonstrated in Sec. II. For such single-qubit gates, the measurement bases of one subsystem are determined by the measurement results of another subsystem. Therefore, implementing a standard one-way logic gate, in general, requires sequential measurements and the feedback of measurement results. In addition, due to the noninstantaneous nature of the measurements, which usually are slower than a CZ gate, the feedback of the measurement results also introduces more errors. In this part, we consider the one-way  $X$ -rotation gate as a concrete example, to demonstrate our method to construct one-way rotation gates with delayed measurements.

Before introducing the delayed-choice one-way  $X$ -rotation gate, we briefly recall how to achieve the standard one-way  $X$ -rotation gate

$$U_x(\alpha) = \begin{pmatrix} \cos(\frac{\alpha}{2}) & -i \sin(\frac{\alpha}{2}) \\ -i \sin(\frac{\alpha}{2}) & \cos(\frac{\alpha}{2}) \end{pmatrix}, \quad (7)$$

with a rotation angle  $\alpha$ . We first initialize the three-qubit system ( $Q_1$ ,  $Q_2$ , and  $Q_3$ ), shown in Fig. 7, in the state

$$|\Phi\rangle_{\text{in}}^x = |\phi\rangle_1 |+_x\rangle_2 |+_x\rangle_3, \quad (8)$$

where  $|\phi\rangle_1$  is the input state of the gate. After the initialization, a cluster state is constructed by applying the CZ gates  $C_Z^{(12)}$  and  $C_Z^{(23)}$  on the system. Then, an  $X$  measurement is performed on  $Q_1$  with outcome  $s_1$ . Now, the measurement basis for  $Q_2$  is determined by  $\eta = (-1)^{s_1+1}\alpha$ . Here,  $\eta$  is the phase angle on the  $xy$  plane of the measurement basis. As we can see, the feedback  $s_1$  will decide the measurement basis. Finally,

a feedforward operation

$$U_\Sigma^X = Z_3^{s_1} X_3^{s_2} \quad (9)$$

is applied to  $Q_3$ , changing the state of  $Q_3$  to  $U_x(\alpha)|\phi\rangle_3$ .

In what follows, we apply the delayed-choice method to the one-way  $X$ -rotation gate. The quantum circuit model for the delayed-choice one-way  $X$ -rotation gate is shown in Fig. 8. In the feedforward part, we apply a controlled  $Z$ -rotation gate on  $Q_1$  and  $Q_2$  (denoted by  $CRZ_{12}$  in the following) with an angle  $-2\alpha$ . The subscript 12 corresponds to the control qubit  $Q_1$  and the target qubit  $Q_2$ , respectively. After the  $CRZ_{12}$  gate, we apply a single-qubit  $Z$ -rotation gate  $RZ$  on  $Q_2$  with an angle  $\alpha$ . These two gates generate a superposition state of two eigenstates of the projectors on the  $xy$  plane with the angle  $\eta = \pm\alpha$ . Therefore, the superposed state contains the readout information  $s_1 = 0$  and 1, corresponding to different total rotation angles  $\eta = \alpha$  and  $-\alpha$ .

After measuring  $Q_1$ , the superposed state collapses to the state with the corresponding result  $s_1$ . On the other hand, we also apply the delayed choice to carry out the feedforward operation in Eq. (9). Note that we do not need to replace the swapped qubit, if it is not involved in any further multiqubit operation. In this protocol, one SWAP operation between  $Q_1$  and  $Q_2$  is sufficient, so we do not replace it with ISWAP gates.

Figure 9 shows the results of running the delayed-choice one-way  $X$ -rotation gate on IBMQ Lima with and without measurement-error mitigation. We consider the input on  $Q_1$  to be  $|0\rangle_1$  and the rotation angle is  $\alpha = \pi/2$ . Therefore, the output state is expected to be rotated to  $|_{-y}\rangle_3$ , where  $|_{-y}\rangle$  is the eigenstate of the Pauli  $Y$  matrix with the eigenvalue  $-1$ . We also present the experimental results for other input states in Appendix A. As shown in Fig. 9, the probability of obtaining the expected readout without error mitigation is 0.916, while the mitigated result is 0.952. In addition, we have performed process tomography of the one-way  $X$ -rotation gate and obtained a gate fidelity of 0.964 (0.948) with (without) error mitigation.

The delayed-choice  $X$ -rotation gate requires eight CNOT gates and three physical qubits. Using the aforementioned error analysis in Sec. II B, the error rate introduced by pure dephasing and energy dissipation is approximately 1.5%. Moreover, the eight CNOT gates for the one-way  $X$ -rotation gate combined together have a total error rate of approximately 3.5%. Finally, readout error would lead to an additional error rate of approximately 2.6%. Therefore, these three factors of error together would be the main limitations of our delayed-choice one-way  $X$ -rotation gate in these experiments.

Compared to the delayed-choice one-way CNOT gate discussed in Sec. II B, the influence of all the three noise channels on the  $X$ -rotation gate decreases. This is because we avoided using a qubit with poor parameters in the  $X$ -rotation gate case. In the one-way CNOT gate, the relaxation time  $T_1$  and decoherence time  $T_2$  of qubit  $Q_3$  are around  $2/3$ , which is less than for the qubits  $Q_0$ – $Q_2$ , and the readout error of  $Q_3$  is approximately twice as much as the readout error of  $Q_0$ – $Q_2$ . The gate error of two-qubit gates involving  $Q_3$  is also twice the two-qubit gate errors between  $Q_0$  and  $Q_1$ , and also between  $Q_1$  and  $Q_2$ . Since we did not use  $Q_3$  in the delayed-choice one-way  $X$ -rotation gate, the total error rates of all the three

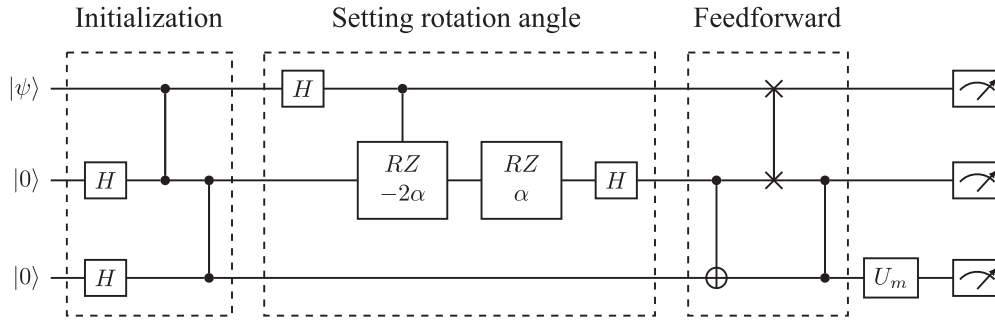


FIG. 8. The circuit for the delayed-choice one-way  $X$ -rotation gate. The input and output states are encoded in qubits  $Q_1$  and  $Q_3$ , respectively. The gate  $U_m$  before measuring qubit  $Q_3$  represents a rotation operation that decides the measurement basis for  $Q_3$ .

noise channels decreased significantly. Our simulation model also supports the above analysis.

#### IV. SUMMARY AND DISCUSSION

In this paper, we have proposed and demonstrated a delayed-choice method to replace the classical conditional operations for realizing deterministic one-way logic gates. Our method can, in general, significantly decrease the impact of readout error and thus increase the fidelity of one-way logic gates. With this simple approach, we can experimentally implement one-way quantum logical gates in noisy intermediate-scale quantum computers, e.g., the IBM Quantum Experience. We presented two explicit examples: (i) a one-way CNOT gate and (ii) a one-way  $X$ -rotation gate.

In our experiments on the IBMQ Lima, we showed how these delayed-choice one-way logic gates perform on currently available devices. We also applied the one-way CNOT gate in the DJ algorithm to demonstrate that our approach can be used in some practical problems. Moreover, we further decreased the gate error by replacing the SWAP gates with ISWAP gates, and decreased measurement errors by applying measurement-error mitigation.

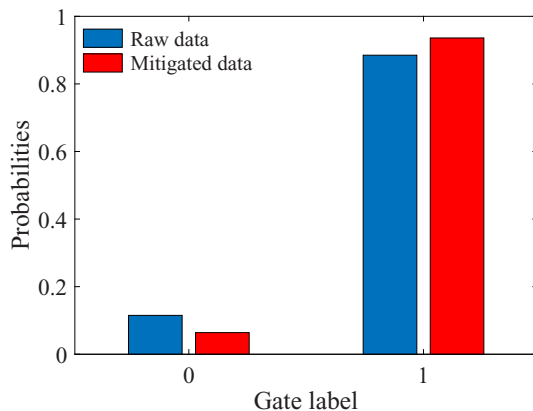


FIG. 9. Experimental results for the delayed-choice one-way  $X$ -rotation gate on IBMQ Lima. The blue and red bars correspond to conditions without and with measurement-error mitigation, respectively. We use the input state  $|0\rangle_1$  and the rotation angle  $\alpha = \pi/2$ . Thus, the output should ideally be  $|{-y}\rangle_3$ , and this is what the measurement result 1 will correspond to.

Comparing to standard one-way logic gates, which only require a series of single-qubit measurements after preparing the cluster states, our protocols additionally imported a series of ancilla single-qubit and two-qubit logic gates, which makes the protocol more complex. However, as we mentioned above, the delayed-choice approach generates a superposition of eigenstates and collapses to the required eigenstate after the measurement operations. With this simple relaxation, we can demonstrate basic one-way quantum computing in superconducting circuits. Moreover, we note that our delayed-choice proposal can significantly decrease the effect of measurement error. In the original feedforward one-way quantum gates, readouts of all the qubits are required to resolve the feedforward operations. Measurement error of any qubit will result in an incorrect quantum operation and thus bring unreliable feedforward operations. However, our delayed-choice proposal only performs the measurements on the ancilla qubits after which the state of the system collapses and the correctness of the measurement results is not critical. Thus, in our delayed-choice proposal, the measurement errors on the ancilla qubits do not affect the fidelity of the one-way logical gate.

As we have discussed in Secs. II and III, the performance of delayed-choice one-way gates is mainly affected by qubit decoherence, gate error, and measurement error. In addition, one-way quantum computing is also limited by the scale of the cluster state we can construct, and currently the largest available superconducting quantum device contains only several dozen qubits [46,50,80]. For practical applications, it is desirable to have more qubits, and future quantum devices are planned with many more qubits.

Finally, it would be interesting to complete universal one-way quantum gates, especially the remaining one-Hadamard and one-way single-qubit arbitrary rotation gates. However, due to the limitation of IBMQ Lima, many SWAP gates need to be inserted into the circuit models, such that the circuit depth

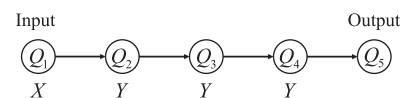


FIG. 10. The basic idea of the one-way Hadamard gate. The qubits  $Q_1$  and  $Q_5$  are the input and output qubits, respectively. The  $X$  or  $Y$  under each qubit represents the measurement basis used for those qubits.



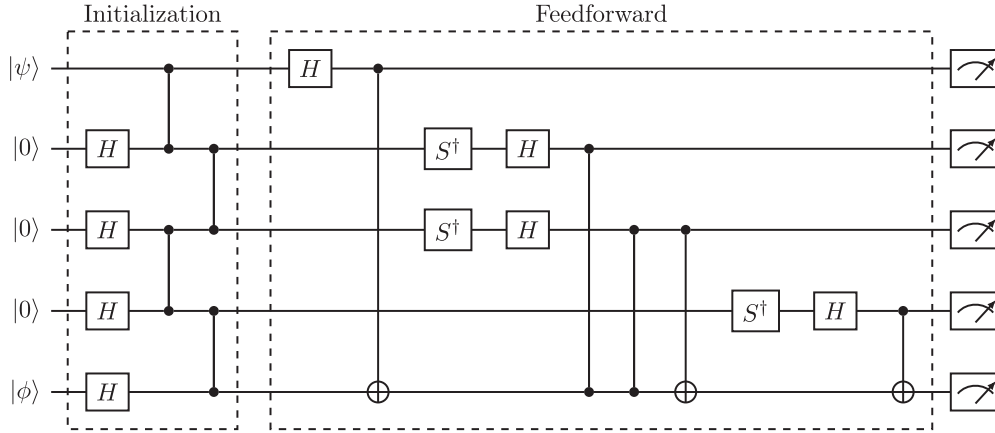


FIG. 11. The circuit for the delayed-choice one-way Hadamard gate. The input and output states are encoded in qubits  $Q_1$  and  $Q_5$ , respectively. This circuit did not consider physical connectivity between qubits in actual hardware.

increases drastically. We have presented details of the circuit models and the simulation results in Appendices B and C.

**ACKNOWLEDGMENTS**

We acknowledge the IBM Quantum Experience for providing us a platform to implement the experiment. We also acknowledge fruitful discussions with R. Wang, Y. Zhou, D.-K. Zhang, S. Devitt, Z.-Q. Yin, S.-L. Ma, Y. Xu, H. Mukai, and S. Shirai. Z.-P.Y. acknowledges the support of China Scholarship Council. Z.-P.Y. and F.-L.L. were in part supported by the National Nature Science Foundation of China (Grant No. 12074307). H.-Y.K. acknowledges the support of the Ministry of Science and Technology, Taiwan (MOST Grant No. 110-2811-M-006-546). Y.-R.Z. acknowledges the Japan Society for the Promotion of Science (JSPS) (via Postdoctoral Fellowship Grant No. P19326 and KAKENHI Grant No. JP19F19326). A.F.K. acknowledges support from the Japan Society for the Promotion of Science (BRIDGE Fellowship No. BR190501), the Swedish Research Council (Grant No. 2019-03696), and the Knut and Alice Wallenberg Foundation through the Wallenberg Centre for Quantum Technology. Y.-N.C. is supported partially by the National Center for Theoretical Sciences and Ministry of Science and Technology, Taiwan, MOST Grant No. 110-2123-M-006-001, and ARO Grant No. W911NF-19-1-0081. J.T. acknowledges support from Japan Science and Technology Agency (JST, via Moonshot R&D Grant No. JPMJMS2067 and CREST Grant No. JPMJCR1676) and the New Energy and Industrial Technology Development Organization, Japan (Grant No. JPNP16007). F.N. is supported in part by Nippon Telegraph and Telephone Corporation Research, JST

(via the Quantum Leap Flagship Program, Moonshot R&D Grant No. JPMJMS2061, and Centers of Research Excellence in Science and Technology Grant No. JPMJCR1676), JSPS [via Grants-in-Aid for Scientific Research KAKENHI Grant No. JP20H00134, ARO Grant No. W911NF-18-1-0358, Asian Office of Aerospace Research and Development Grant No. FA2386-20-1-4069, and Foundational Questions Institute Fund Grant No. FQXi-IAF19-06.

**APPENDIX A: DETAILED DATA OBTAINED FROM IBMQ FOR THE DELAYED-CHOICE ONE-WAY CNOT AND X-ROTATION GATES**

In this Appendix, we first present the detailed data for the one-way logic gates that we ran on IBMQ Lima. The experimental data of the delayed-choice one-way CNOT gates and the delayed-choice one-way X-rotation gate are presented in Tables I and II, respectively. The parameters which we used in our simulation model are presented in Table III.

**APPENDIX B: DELAYED-CHOICE PROTOCOL FOR THE ONE-WAY HADAMARD GATE**

In this section, we introduce a protocol to construct a one-way Hadamard gate by utilizing the delayed-choice approach. We also show the simulation results we obtained on the quantum assembly simulator for this protocol.

The original idea for the one-way Hadamard gate is shown in Fig. 10. The one-way Hadamard gate requires five physical qubits, labeled  $Q_1$  to  $Q_5$ .  $Q_1$  serves as the input qubit, while

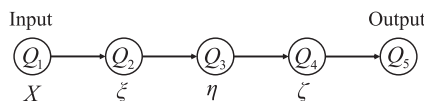


FIG. 12. The basic idea of the one-way arbitrary rotation gate. The qubits  $Q_1$  and  $Q_5$  are the input and output qubits, respectively. The  $X$ ,  $\xi$ ,  $\eta$ , and  $\zeta$  under qubits  $Q_1$  to  $Q_4$  represent the measurement directions of the corresponding qubits.

TABLE II. Probability distribution for the delayed-choice one-way X-rotation gate on IBMQ Lima. Here,  $|\pm_y\rangle$  denotes the Y measurement with the corresponding outcome  $\pm 1$ .

Input $ 0\rangle$	$ +_y\rangle$	$ -_y\rangle$
Raw	0.084	0.916
Mitigated	0.048	0.952
Input $ 1\rangle$	$ +_y\rangle$	$ -_y\rangle$
Raw	0.926	0.074
Mitigated	0.932	0.068

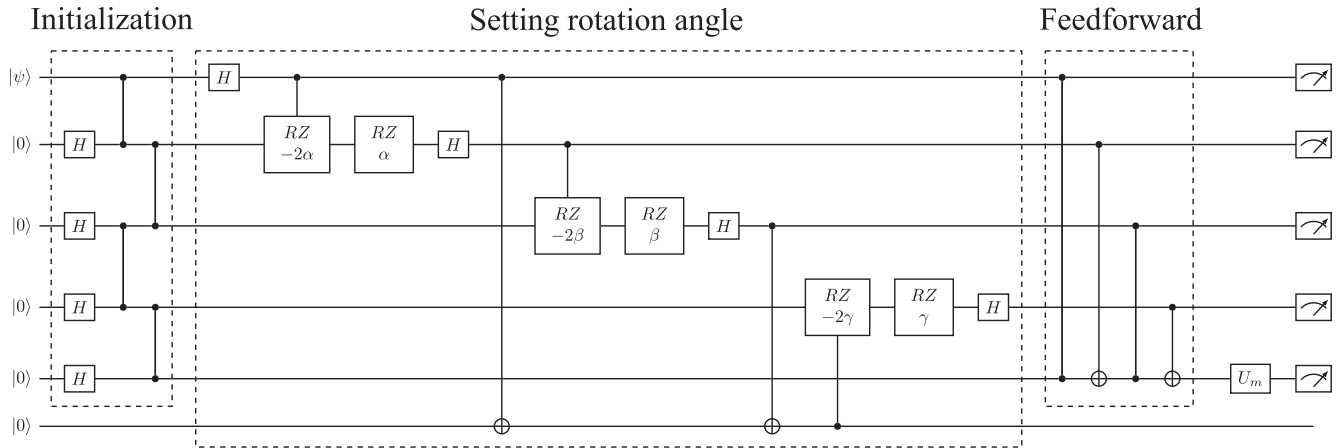


FIG. 13. The circuit for the delayed-choice one-way arbitrary rotation gate. The input and output states are encoded in qubits  $Q_1$  and  $Q_5$ , respectively. The gate  $U_m$  before measuring qubit  $Q_5$  represents a rotation operation that decides the measurement basis for  $Q_5$ .

the other four qubits are initialized in the state  $|+_x\rangle$ . After constructing a linear cluster state on these five qubits by carrying out CZ gates  $C_Z^{(12)}$ ,  $C_Z^{(23)}$ ,  $C_Z^{(34)}$ , and  $C_Z^{(45)}$ , qubit  $Q_1$  is measured in the  $X$  basis, while qubits  $Q_2$ ,  $Q_3$ , and  $Q_4$  are measured in the  $Y$  basis. These measurement operations can be carried out simultaneously, and we denote the measurement results  $s_1$  to  $s_4$ , respectively. Finally, a feedforward operation  $U_\Sigma^H = X^{s_1+s_3+s_4} Z^{s_2+s_3}$  is applied to the output qubit  $Q_5$ , and the output state corresponding to the Hadamard gate having acted on the input state is obtained.

Similar to the one-way CNOT gate, we can also apply the delayed-choice approach to carry out a one-way Hadamard gate on the IBMQ devices. The logical circuit of our one-way Hadamard gate is shown in Fig. 11. We note that this circuit does not take system connectivity into consideration. In the real device, we need to apply SWAP or ISWAP gates in order to demonstrate the quantum operations between non-neighboring qubits.

The simulation results for our one-way Hadamard gate, obtained on the quantum assembly simulator, are shown in Table IV. We not only consider the ideal case in which there is no noise in the circuit, but also perform simulations including noise corresponding to single-qubit and two-qubit gate fidelities of 99.8 and 98 %, respectively. These gate errors are higher than those of IBMQ Lima. The results for the noisy case do not show very high fidelity, but are clear enough to correctly identify the logical output.

TABLE III. Noise parameters of the IBMQ Lima. Qubits  $Q_0$ ,  $Q_1$ ,  $Q_2$ , and  $Q_3$  are utilized in the delayed-choice one-way CNOT gate, while  $Q_0$ ,  $Q_1$ , and  $Q_2$  are involved in the delayed-choice one-way  $X$ -rotation gate.

Qubits	$T_1$ ( $\mu$ s)	$T_2$ ( $\mu$ s)	$\lambda_{01}$	$\lambda_{10}$	Pauli- $X$ error ( $\times 10^{-4}$ )
$Q_0$	152.60	192.19	0.0252	0.0094	1.96
$Q_1$	114.79	106.56	0.0230	0.0034	2.20
$Q_2$	108.53	109.94	0.0304	0.0060	2.18
$Q_3$	85.16	69.66	0.0474	0.0168	2.79
$Q_4$	18.24	17.71	0.1112	0.0176	7.16

We also attempted to implement our circuit directly on IBMQ Lima, but the experimental results were clearly worse than the simulations had indicated and are not shown here. In order to realize a delayed-choice one-way Hadamard gate in IBMQ Lima, we need to apply at least six SWAP gates. In other words, it requires at least 27 CNOT gates, which is over twice that in the delayed-choice one-way CNOT gate. Such a large circuit depth gives decoherence too much time to destroy the quantum state.

### APPENDIX C: DELAYED-CHOICE PROTOCOL FOR ONE-WAY ARBITRARY SINGLE-QUBIT ROTATIONS

The delayed-choice approach can also be utilized to construct a one-way arbitrary rotation gate, achieving a universal one-way logic gate set together with the one-way CNOT gate shown in Sec. II. However, due to the limitations of the IBMQ devices, we were unable to obtain satisfying results on any real device. In this section, we therefore demonstrate the delayed-choice one-way arbitrary rotation gate with the quantum assembly simulator.

The basic principle of a one-way arbitrary rotation gate  $U_{\text{rot}}(\xi, \eta, \zeta) = U_x(\zeta)U_z(\eta)U_x(\xi)$  is shown in Fig. 12, where

TABLE IV. Probability distribution for the delayed-choice one-way Hadamard gate on the quantum assembly simulator. This circuit is designed for IBMQ Lima. This table shows the simulation results under two conditions: (a) ideal conditions without noise and (b) conditions with noise, using SWAP gates in the circuit in Fig. 11 to compensate for the limited qubit connectivity. For condition (b), the fidelities of the single-qubit and two-qubit gates are set to 99.8 and 98 %, respectively.

Input $ +_x\rangle$	$ 0\rangle$	$ 1\rangle$
Ideal	1	0
Noisy	0.825	0.175
Input $ -_x\rangle$	$ 0\rangle$	$ 1\rangle$
Ideal	0	1
Noisy	0.185	0.815

TABLE V. Probability distribution for the delayed-choice one-way arbitrary rotation gate  $U_{\text{rot}}(\xi, \eta, \zeta) = U_x(\zeta)U_z(\eta)U_x(\xi)$  on the quantum assembly simulator. This circuit does not consider the actual qubit connectivity, but instead assumes that all the qubits can directly interact with each other as required. This table shows the simulation results with different rotation angles. During the simulation, we have considered two inputs with different rotation angles: (a) input state  $|\psi\rangle = |0\rangle$  with rotation angles  $(\frac{\pi}{2}, \frac{\pi}{2}, 0)$  and (b) input state  $|\psi\rangle = |+_y\rangle$  with rotation angles  $(0, \pi, \frac{\pi}{2})$ . For the simulations with noise, the fidelities of the single-qubit and two-qubit gates are set to 99.8 and 98 %, respectively.

Input $ 0\rangle$ , angle $(\frac{\pi}{2}, \frac{\pi}{2}, 0)$	$ +_x\rangle$	$ -_x\rangle$
Ideal	1	0
Noisy	0.866	0.134
Input $ +_y\rangle$ , angle $(0, \pi, \frac{\pi}{2})$	$ 0\rangle$	$ 1\rangle$
Ideal	0	1
Noisy	0.137	0.863

$U_a(\theta)$  represents a rotation operation about the  $a$  axis ( $a = x, z$ ) with rotation angle  $\theta$ . This gate is implemented using five physical qubits, labeled  $Q_1$  to  $Q_5$ . Similar to the one-way  $X$ -rotation gate,  $Q_1$  is the input qubit, while  $Q_2$  to  $Q_5$  are

initialized in the state  $|+_x\rangle$ . After entangling the qubits with CZ gates  $C_Z^{(12)}$ ,  $C_Z^{(23)}$ ,  $C_Z^{(34)}$ , and  $C_Z^{(45)}$ , qubit  $Q_1$  is measured in the  $X$  basis, yielding the result  $s_1$ . After this, measurements on qubits  $Q_2$ ,  $Q_3$ , and  $Q_4$  are carried out in sequence, giving the corresponding results  $s_2$ ,  $s_3$ , and  $s_4$ . Here, the measurement bases are in the  $xy$  plane, with the angles to the  $x$  axis  $\alpha = (-1)^{s_1}\xi$ ,  $\beta = (-1)^{s_2}\eta$ , and  $\gamma = (-1)^{s_1+s_3}\zeta$ . Finally, a feedforward operation  $U_{\Sigma}^{\text{rot}} = Z_5^{s_1+s_3}X_5^{s_2+s_4}$  is carried out on qubit  $Q_5$ , which then ends up in the state corresponding to applying  $U_{\text{rot}}(\xi, \eta, \zeta)$  on the input state.

We note that the measurement direction of qubit  $Q_4$  is determined by both the measurement results  $s_1$  and  $s_3$ , which makes it impossible to apply delayed choice directly. In order to solve this, we bring in another physical qubit as a register that calculates and saves the Boolean result  $s_1 + s_3$ . This additional qubit also serves as the control qubit during the corresponding delayed choice. The delayed-choice one-way arbitrary rotation gate is shown in Fig. 13. Here, the delayed-choice one-way arbitrary rotation gate requires more SWAP operations than the Hadamard case. Due to the aforementioned analysis, we are simply trying to show the logical result of our protocol.

The results of our numerical simulations are shown in Table V. For the noisy simulations, we used the same parameters as in the simulations in Appendix B.

- 
- [1] R. Raussendorf and H. J. Briegel, A One-Way Quantum Computer, *Phys. Rev. Lett.* **86**, 5188 (2001).
- [2] R. Raussendorf, D. E. Browne, and H. J. Briegel, Measurement-based quantum computation on cluster states, *Phys. Rev. A* **68**, 022312 (2003).
- [3] H. J. Briegel, D. E. Browne, W. Dür, R. Raussendorf, and M. Van den Nest, Measurement-based quantum computation, *Nat. Phys.* **5**, 19 (2009).
- [4] H. J. Briegel and R. Raussendorf, Persistent Entanglement in Arrays of Interacting Particles, *Phys. Rev. Lett.* **86**, 910 (2001).
- [5] O. Gühne and G. Tóth, Entanglement detection, *Phys. Rep.* **474**, 1 (2009).
- [6] M. Zwerger, H. J. Briegel, and W. Dür, Universal and Optimal Error Thresholds for Measurement-Based Entanglement Purification, *Phys. Rev. Lett.* **110**, 260503 (2013).
- [7] M. Zwerger, H. J. Briegel, and W. Dür, Hybrid architecture for encoded measurement-based quantum computation, *Sci. Rep.* **4**, 5364 (2015).
- [8] R. Harper and S. T. Flammia, Fault-Tolerant Logical Gates in the IBM Quantum Experience, *Phys. Rev. Lett.* **122**, 080504 (2019).
- [9] J. Hastrup, K. Park, J. B. Brask, R. Filip, and U. L. Andersen, Measurement-free preparation of grid states, *npj Quantum Inf.* **7**, 17 (2021).
- [10] R. Raussendorf, J. Harrington, and K. Goyal, A fault-tolerant one-way quantum computer, *Ann. Phys. (NY)* **321**, 2242 (2006).
- [11] M. Varnava, D. E. Browne, and T. Rudolph, Loss Tolerance in One-Way Quantum Computation via Counterfactual Error Correction, *Phys. Rev. Lett.* **97**, 120501 (2006).
- [12] D. Herr, A. Paler, S. J. Devitt, and F. Nori, Lattice surgery on the Raussendorf lattice, *Quantum Sci. Technol.* **3**, 035011 (2018).
- [13] R. R. Ferguson, L. Dellantonio, A. A. Balushi, K. Jansen, W. Dür, and C. A. Muschik, Measurement-Based Variational Quantum Eigensolver, *Phys. Rev. Lett.* **126**, 220501 (2021).
- [14] W. Asavanant, Y. Shiozawa, S. Yokoyama, B. Charoensombutamon, H. Emura, R. N. Alexander, S. Takeda, J. Yoshikawa, N. C. Menicucci, H. Yonezawa, and A. Furusawa, Generation of time-domain-multiplexed two-dimensional cluster state, *Science* **366**, 373 (2019).
- [15] M. V. Larsen, X. Guo, C. R. Breum, J. S. Neergaard-Nielsen, and U. L. Andersen, Deterministic generation of a two-dimensional cluster state, *Science* **366**, 369 (2019).
- [16] R. Vasconcelos, S. Reisenbauer, C. Salter, G. Wachter, D. Wirtitsch, J. Schmiedmayer, P. Walther, and M. Trupke, Scalable spin-photon entanglement by time-to-polarization conversion, *npj Quantum Inf.* **6**, 9 (2020).
- [17] B. Ndagano, H. Defienne, A. Lyons, I. Starshynov, F. Villa, S. Tisa, and D. Faccio, Imaging and certifying high-dimensional entanglement with a single-photon avalanche diode camera, *npj Quantum Inf.* **6**, 94 (2020).
- [18] P. Hilaire, E. Barnes, and S. E. Economou, Resource requirements for efficient quantum communication using all-photonic graph states generated from a few matter qubits, *Quantum* **5**, 397 (2021).
- [19] T. Tanamoto, Y.-x. Liu, S. Fujita, X. Hu, and F. Nori, Producing Cluster States in Charge Qubits and Flux Qubits, *Phys. Rev. Lett.* **97**, 230501 (2006).

- [20] J. Q. You, X.-b. Wang, T. Tanamoto, and F. Nori, Efficient one-step generation of large cluster states with solid-state circuits, *Phys. Rev. A* **75**, 052319 (2007).
- [21] T. Tanamoto, Y.-x. Liu, X. Hu, and F. Nori, Efficient Quantum Circuits for One-Way Quantum Computing, *Phys. Rev. Lett.* **102**, 100501 (2009).
- [22] A. Kay, J. K. Pachos, and C. S. Adams, Graph-state preparation and quantum computation with global addressing of optical lattices, *Phys. Rev. A* **73**, 022310 (2006).
- [23] J. Joo, P. L. Knight, J. L. O'Brien, and T. Rudolph, One-way quantum computation with four-dimensional photonic qudits, *Phys. Rev. A* **76**, 052326 (2007).
- [24] Y. Miwa, J.-i. Yoshikawa, P. van Loock, and A. Furusawa, Demonstration of a universal one-way quantum quadratic phase gate, *Phys. Rev. A* **80**, 050303(R) (2009).
- [25] Y. Wang, X. Su, H. Shen, A. Tan, C. Xie, and K. Peng, Toward demonstrating controlled-X operation based on continuous-variable four-partite cluster states and quantum teleporters, *Phys. Rev. A* **81**, 022311 (2010).
- [26] H. Shen, K. Qu, W. Zhang, and J. Jin, Controlled-X gate with cache function for one-way quantum computation, *Phys. Rev. A* **85**, 032317 (2012).
- [27] B. A. Bell, M. S. Tame, A. S. Clark, R. W. Nock, W. J. Wadsworth, and J. G. Rarity, Experimental characterization of universal one-way quantum computing, *New J. Phys.* **15**, 053030 (2013).
- [28] S. Hao, X. Deng, X. Su, X. Jia, C. Xie, and K. Peng, Gates for one-way quantum computation based on Einstein-Podolsky-Rosen entanglement, *Phys. Rev. A* **89**, 032311 (2014).
- [29] F. Albarrán-Arriagada, G. Alvarado Barrios, M. Sanz, G. Romero, L. Lamata, J. C. Retamal, and E. Solano, One-way quantum computing in superconducting circuits, *Phys. Rev. A* **97**, 032320 (2018).
- [30] P. Walther, K. J. Resch, T. Rudolph, E. Schenck, H. Weinfurter, V. Vedral, M. Aspelmeyer, and A. Zeilinger, Experimental one-way quantum computing, *Nature (London)* **434**, 169 (2005).
- [31] N. Kiesel, C. Schmid, U. Weber, G. Tóth, O. Gühne, R. Ursin, and H. Weinfurter, Experimental Analysis of a Four-Qubit Photon Cluster State, *Phys. Rev. Lett.* **95**, 210502 (2005).
- [32] R. Prevedel, P. Walther, F. Tiefenbacher, P. Böhi, R. Kaltenbaek, T. Jennewein, and A. Zeilinger, High-speed linear optics quantum computing using active feed-forward, *Nature (London)* **445**, 65 (2007).
- [33] M. S. Tame, R. Prevedel, M. Paternostro, P. Böhi, M. S. Kim, and A. Zeilinger, Experimental Realization of Deutsch's Algorithm in a One-Way Quantum Computer, *Phys. Rev. Lett.* **98**, 140501 (2007).
- [34] K. Chen, C.-M. Li, Q. Zhang, Y.-A. Chen, A. Goebel, S. Chen, A. Mair, and J.-W. Pan, Experimental Realization of One-Way Quantum Computing with Two-Photon Four-Qubit Cluster States, *Phys. Rev. Lett.* **99**, 120503 (2007).
- [35] G. Vallone, E. Pomarico, F. De Martini, and P. Mataloni, Active One-Way Quantum Computation with Two-Photon Four-Qubit Cluster States, *Phys. Rev. Lett.* **100**, 160502 (2008).
- [36] R. Kaltenbaek, J. Lavoie, B. Zeng, B. S. D., and K. J. Resch, Optical one-way quantum computing with a simulated valence-bond solid, *Nat. Phys.* **6**, 850 (2010).
- [37] M. S. Tame, B. A. Bell, C. Di Franco, W. J. Wadsworth, and J. G. Rarity, Experimental Realization of a One-Way Quantum Computer Algorithm Solving Simon's Problem, *Phys. Rev. Lett.* **113**, 200501 (2014).
- [38] B. P. Lanyon, P. Jurcevic, M. Zwerger, C. Hempel, E. A. Martinez, W. Dür, H. J. Briegel, R. Blatt, and C. F. Roos, Measurement-Based Quantum Computation with Trapped Ions, *Phys. Rev. Lett.* **111**, 210501 (2013).
- [39] C. Ju, J. Zhu, X. Peng, B. Chong, X. Zhou, and J.-F. Du, Experimental demonstration of deterministic one-way quantum computation on a NMR quantum computer, *Phys. Rev. A* **81**, 012322 (2010).
- [40] J.-Q. You and F. Nori, Atomic physics and quantum optics using superconducting circuits, *Nature (London)* **474**, 589 (2011).
- [41] I. Buluta, S. Ashhab, and F. Nori, Natural and artificial atoms for quantum computation, *Rep. Prog. Phys.* **74**, 104401 (2011).
- [42] X. Gu, A. F. Kockum, A. Miranowicz, Y.-x. Liu, and F. Nori, Microwave photonics with superconducting quantum circuits, *Phys. Rep.* **718-719**, 1 (2017).
- [43] A. F. Kockum and F. Nori, Quantum bits with Josephson junctions, in *Fundamentals and Frontiers of the Josephson Effect*, edited by F. Tafuri (Springer, New York, 2019), pp. 703–741.
- [44] M. Kjaergaard, M. E. Schwartz, J. Braumüller, P. Krantz, J. I.-J. Wang, S. Gustavsson, and W. D. Oliver, Superconducting Qubits: Current State of Play, *Annu. Rev. Condens. Matter Phys.* **11**, 369 (2020).
- [45] D. R. W. Yost, M. E. Schwartz, J. Mallek, D. Rosenberg, C. Stull, J. L. Yoder, G. Calusine, M. Cook, R. Das, A. L. Day, E. B. Golden, D. K. Kim, A. Melville, B. M. Niedzielski, W. Woods, A. J. Kerman, and W. D. Oliver, Solid-state qubits integrated with superconducting through-silicon vias, *npj Quantum Inf.* **6**, 59 (2020).
- [46] IBM Quantum Experience, <https://quantum-computing.ibm.com/>.
- [47] A. Kandala, A. Mezzacapo, K. Temme, M. Takita, M. Brink, J. M. Chow, and J. M. Gambetta, Hardware-efficient variational quantum eigensolver for small molecules and quantum magnets, *Nature (London)* **549**, 242 (2017).
- [48] A. Kandala, K. Temme, A. D. Córcoles, A. Mezzacapo, J. M. Chow, and J. M. Gambetta, Error mitigation extends the computational reach of a noisy quantum processor, *Nature (London)* **567**, 491 (2019).
- [49] A. Chiesa, F. Tacchino, M. Grossi, P. Santini, I. Tavernelli, D. Gerace, and S. Carretta, Quantum hardware simulating four-dimensional inelastic neutron scattering, *Nat. Phys.* **15**, 455 (2019).
- [50] F. Arute *et al.*, Quantum supremacy using a programmable superconducting processor, *Nature (London)* **574**, 505 (2019).
- [51] C. Neill *et al.*, Accurately computing the electronic properties of a quantum ring, *Nature (London)* **594**, 508 (2021).
- [52] X. L. Zhang, K. L. Gao, and M. Feng, Preparation of cluster states and  $W$  states with superconducting quantum-interference-device qubits in cavity QED, *Phys. Rev. A* **74**, 024303 (2006).
- [53] G. Chen, Z. Chen, L. Yu, and J. Liang, One-step generation of cluster states in superconducting charge qubits coupled with a nanomechanical resonator, *Phys. Rev. A* **76**, 024301 (2007).
- [54] Z. Li, S.-I. Ma, Z.-p. Yang, A.-p. Fang, P.-b. Li, S.-y. Gao, and F.-I. Li, Generation and replication of continuous-variable quadripartite cluster and Greenberger-Horne-Zeilinger states in

- four chains of superconducting transmission line resonators, *Phys. Rev. A* **93**, 042305 (2016).
- [55] P. Lähteenmäki, G. S. Paraoanu, J. Hassel, and P. J. Hakonen, Coherence and multimode correlations from vacuum fluctuations in a microwave superconducting cavity, *Nat. Commun.* **7**, 12548 (2016).
- [56] Z.-p. Yang, Z. Li, S.-l. Ma, and F.-l. Li, One-step generation of continuous-variable quadripartite cluster states in a circuit QED system, *Phys. Rev. A* **96**, 012327 (2017).
- [57] Y. Wang, Y. Li, Z.-q. Yin, and B. Zeng, 16-qubit IBM universal quantum computer can be fully entangled, *npj Quantum Inf.* **4**, 46 (2018).
- [58] M. Gong, M.-C. Chen, Y. Zheng, S. Wang, C. Zha, H. Deng, Z. Yan, H. Rong, Y. Wu, S. Li, F. Chen, Y. Zhao, F. Liang, J. Lin, Y. Xu, C. Guo, L. Sun, A. D. Castellano, H. Wang, C. Peng *et al.*, Genuine 12-Qubit Entanglement on a Superconducting Quantum Processor, *Phys. Rev. Lett.* **122**, 110501 (2019).
- [59] H.-Y. Ku, N. Lambert, F.-J. Chan, C. Emary, Y.-N. Chen, and F. Nori, Experimental test of non-macrorealistic cat states in the cloud, *npj Quantum Inf.* **6**, 98 (2020).
- [60] J.-C. Besse, K. Reuer, M. C. Collodo, A. Wulff, L. Wernli, A. Copetudo, D. Malz, P. Magnard, A. Akin, M. Gabureac, G. J. Norris, J. I. Cirac, A. Wallraff, and C. Eichler, Realizing a deterministic source of multipartite-entangled photonic qubits, *Nat. Commun.* **11**, 4877 (2020).
- [61] S. Shirai, Y. Zhou, K. Sakata, H. Mukai, and J.-S. Tsai, Generating time-domain linear cluster state by recycling superconducting qubits, [arXiv:2105.08609](https://arxiv.org/abs/2105.08609).
- [62] A. Smith, M. S. Kim, F. Pollmann, and J. Knolle, Simulating quantum many-body dynamics on a current digital quantum computer, *npj Quantum Inf.* **5**, 106 (2019).
- [63] G. García-Pérez, M. A. C. Rossi, and S. Maniscalco, IBM Q Experience as a versatile experimental testbed for simulating open quantum systems, *npj Quantum Inf.* **6**, 1 (2020).
- [64] G. A. L. White, C. D. Hill, F. A. Pollock, L. C. L. Hollenberg, and K. Modi, Demonstration of non-Markovian process characterisation and control on a quantum processor, *Nat. Commun.* **11**, 6301 (2020).
- [65] Y.-T. Huang, J.-D. Lin, H.-Y. Ku, and Y.-N. Chen, Benchmarking quantum state transfer on quantum devices, *Phys. Rev. Research* **3**, 023038 (2021).
- [66] S. J. Devitt, Performing quantum computing experiments in the cloud, *Phys. Rev. A* **94**, 032329 (2016).
- [67] S. Woerner and D. J. Egger, Quantum risk analysis, *npj Quantum Inf.* **5**, 15 (2019).
- [68] F. Tacchino, C. Macchiavello, D. Gerace, and D. Bajoni, An artificial neuron implemented on an actual quantum processor, *npj Quantum Inf.* **5**, 26 (2019).
- [69] K. Yeter-Aydeniz, R. C. Pooser, and G. Siopsis, Practical quantum computation of chemical and nuclear energy levels using quantum imaginary time evolution and Lanczos algorithms, *npj Quantum Inf.* **6**, 63 (2020).
- [70] G. J. Mooney, G. A. L. White, C. D. Hill, and L. C. L. Hollenberg, Whole-device entanglement in a 65-qubit superconducting quantum computer, *Adv. Quantum Technol.* **4**, 2100061 (2021).
- [71] A. D. Córcoles, M. Takita, K. Inoue, S. Lekuch, Z. K. Mineev, J. M. Chow, and J. M. Gambetta, Exploiting Dynamic Quantum Circuits in a Quantum Algorithm with Superconducting Qubits, *Phys. Rev. Lett.* **127**, 100501 (2021).
- [72] D. Deutsch, Quantum theory, the Church-Turing principle and the universal quantum computer, *Proc. R. Soc. A* **400**, 97 (1985).
- [73] D. Deutsch and R. Jozsa, Rapid solution of problems by quantum computation, *Proc. R. Soc. A* **439**, 553 (1992).
- [74] Y. Chen, M. Farahzad, S. Yoo, and T.-C. Wei, Detector tomography on ibm quantum computers and mitigation of an imperfect measurement, *Phys. Rev. A* **100**, 052315 (2019).
- [75] S. Dogra, A. Melnikov, and G. Paraoanu, Quantum simulation of parity-time symmetry breaking with a superconducting quantum processor, *Commun. Phys.* **4**, 26 (2021).
- [76] F. B. Maciejewski, Z. Zimborás, and M. Oszmaniec, Mitigation of readout noise in near-term quantum devices by classical post-processing based on detector tomography, *Quantum* **4**, 257 (2020).
- [77] P. Suchsland, F. Tacchino, M. H. Fischer, T. Neupert, P. K. Barkoutsos, and I. Tavernelli, Algorithmic Error Mitigation Scheme for Current Quantum Processors, *Quantum* **5**, 492 (2021).
- [78] E. Magesan, J. M. Gambetta, and J. Emerson, Scalable and Robust Randomized Benchmarking of Quantum Processes, *Phys. Rev. Lett.* **106**, 180504 (2011).
- [79] E. Magesan, J. M. Gambetta, and J. Emerson, Characterizing quantum gates via randomized benchmarking, *Phys. Rev. A* **85**, 042311 (2012).
- [80] Y. Wu *et al.*, Strong Quantum Computational Advantage Using a Superconducting Quantum Processor, *Phys. Rev. Lett.* **127**, 180501 (2021).